Taylor & Francis
Taylor & Francis Group

Nitrogen-doped carbon quantum dot regulates cell proliferation and differentiation by endoplasmic reticulum stress

Hyun Hee Song[a], Hyunwoo Choi[b], Seonghan Kim[c], Hwan Gyu Kim[a]*, Sangmin An[e]*, Sejung Kim[c,d]* and Hoon Jang [a,f]*

[a]Department of Life Science, Jeonbuk National University, Jeonju, Republic of Korea; [b]Department of Animal Science, Jeonbuk National University, Jeonju, Republic of Korea; [c]School of Chemical Engineering, Clean Energy Research Center, Jeonbuk National University, Jeonju, Republic of Korea; [d]Department of JBNU-KIST Industry-Academia Convergence Research, Jeonbuk National University, Jeonju, Republic of Korea; [e]Department of Physics, Jeonbuk National University, Jeonju, Republic of Korea; [f]Quantabiom Co., Ltd., Jeonju, Republic of Korea

ABSTRACT
Quantum dots have diverse biomedical applications, from constructing biological infrastructures like medical imaging to advancing pharmaceutical research. However, concerns about human health arise due to the toxic potential of quantum dots based on heavy metals. Therefore, research on quantum dots has predominantly focused on oxidative stress, cell death, and other broader bodily toxicities. This study investigated the toxicity and cellular responses of mouse embryonic stem cells (mESCs) and mouse adult stem cells (mASCs) to nitrogen-doped carbon quantum dots (NCQDs) made of non-metallic materials. Cells were exposed to NCQDs, and we utilized a fluorescent ubiquitination-based cell system to verify whether NCQDs induce cytotoxicity. Furthermore, we validated the differentiation-inducing impact of NCQDs by utilizing embryonic stem cells equipped with the Oct4 enhancer-GFP reporter system. By analyzing gene expression including Crebzf, Chop, and ATF6, we also observed that NCQDs robustly elicited endoplasmic reticulum (ER) stress. We confirmed that NCQDs induced cytotoxicity and abnormal differentiation. Interestingly, we also confirmed that low concentrations of NCQDs stimulated cell proliferation in both mESCs and mASCs. In conclusion, NCQDs modulate cell death, proliferation, and differentiation in a concentration-dependent manner. Indiscriminate biological applications of NCQDs have the potential to cause cancer development by affecting normal cell division or to fail to induce normal differentiation by affecting embryonic development during pregnancy. Therefore, we propose that future biomedical applications of NCQDs necessitate comprehensive and diverse biological studies.

1. Introduction

Carbon quantum dots (CQDs) are graphene-based nanomaterials similar to oxidized graphitic derivative oxide in terms of their structural and physical properties (Banerjee and Wong 2003). CQDs can be widely used in biological applications such as biosensors, cell labeling, cancer targeting, and disease diagnosis because of their luminescence, electronic properties, chemical stability, and water solubility (Chen et al. 2013; Ji et al. 2016; Mansuriya and Altintas 2020). Since the isolation of graphene in 2003, research related to graphene has experienced a global resurgence, with anticipated sales surpassing $300 million by 2024 (Ku et al. 2021). The

widespread utilization of CQDs has the potential to significantly impact living organisms. Small-sized CQDs can persist for a relatively long time in high salinity water or barren desert environments spread to a wide range of environments and cause uncertain biological effects (Akhavan et al. 2012; Dong et al. 2012; Kamrani et al. 2018). Therefore, the biological effects of CQDs require extensive investigation to ensure their safe use in future medical applications. Although several studies have reported the good biocompatibility of CQDs, exposure to some heavy metal-linked QDs or high concentrations of CQDs can cause serious biological side effects such as reactive oxygen species (ROS)

production, DNA cleavage, apoptosis, immune responses, and autophagy in both cells and organisms (Hsieh et al. 2009; Chong et al. 2014; Qin et al. 2015). For example, a recent study reported that oral administration of CQDs in mice caused intestinal injury through the loss of intestinal epithelial progenitor cells (Yu et al. 2019). CQDs have a diameter of approximately ~10 nm, which allows them to easily pass through epithelial cells in the body, allowing them to cross the blood-brain barrier and affect neurons, or even passed on to offspring through germ cells (Huang et al. 2017; Zhang et al. 2019; Wang et al. 2022). Nevertheless, extensive investigation is required to understand how CQDs affect the activation and development of cells.

The endoplasmic reticulum (ER) is a crucial organelle within cells, playing a pivotal role in various cellular functions, including protein synthesis, post-translational modifications (PTMs), cell membrane formation, and the transport of secreted proteins (Schröder and Kaufman 2005b; Cao and Kaufman 2012). Maintaining proper ER function is essential for cellular health (Kwon et al. 2023). However, disruption of ER homeostasis, whether from internal or external factors, can lead to problems such as misfolded proteins or abnormal PTMs in synthesized proteins, which can reduce their biological activity. Accumulation of misfolded proteins inside the ER triggers ER stress, initiating of the unfolded protein response (UPR) (Schröder and Kaufman 2005a; Chakrabarti et al. 2011). The UPR is a complex signaling pathway aimed at restoring ER function by inhibiting protein synthesis, enhancing protein refolding activities, and promoting the degradation of accumulated proteins that cannot be corrected. Three major signaling pathways constitute the UPR: Protein Kinase R-like ER Kinase (PERK)/eIF2a/CHOP (Rozpedek et al. 2016), activating transcription factor 6 (ATF6)/chaperone (Adachi et al. 2008), and inositol requiring enzyme type 1 (Ire1)/xbp1 (Zhou et al. 2021; Lee et al. 2022). Recent studies have also linked ER stress to Crebzf, a protein involved in regulating cell differentiation (Zhang et al. 2013; Jang et al. 2014). Understanding the relationship between ER stress and these proteins is vital for comprehending cellular responses, physiological mechanisms in animals, and the development of disease treatments. This knowledge is especially relevant when investigating the effects of new substances like quantum dots (QDs) on living organisms, as it provides insights into potential impacts on ER stress and cellular functions, crucial for ensuring safety and exploring therapeutic applications.

Embryonic stem cells (mESCs), isolated from the inner cell mass of a developing blastocyst, have revolutionized the study of early mammalian embryonic development, offering valuable insights into processes like organoid formation. Researchers have delved into the intricate regulation of mESCs proliferation and differentiation, uncovering a multitude of mechanisms. Among these, endoplasmic reticulum (ER) stress emerges as a critical player in maintaining the survival and pluripotency of ESCs and influencing their differentiation (Blanco-Gelaz et al. 2010; Kratochvilova et al. 2016; Caballano-Infantes et al. 2017). OG2 cells, which are oct4-enhancer-GFP transgenic ESCs, serve as an efficient system for studying ESC differentiation, as they express GFP when pluripotent (Boiani et al. 2002). ER stress is not limited to mESCs; it also holds significance in the proliferation and differentiation of adult stem cells (ASCs), such as mesenchymal-derived stem cells or neural stem cells (Kurosawa et al. 2007; Kim et al. 2018; Meijer et al. 2021). MC3T3-E1 cell, derived from mouse embryonic osteoblast precursor cells, are a type of ASC extensively employed to assess the effects of biomaterials due to their osteogenic potential (Vimalraj 2020). These cells contribute to the formation of skeletal tissue and play a pivotal role in tissue regeneration when injury or damage occurs, making them highly sensitive to ER stress during osteoblast differentiation (Jang et al. 2014). ER stress can be triggered by various substances and research has reported on the ER stress inducing effects of quantum dots (QDs) doped with heavy metals or minerals (Wang et al. 2015; Yan et al. 2016; Bai et al. 2022; Zhang et al. 2023). While some studies have explored the impact of graphene QDs on ESC differentiation through genome methylation regulation (Ku et al. 2021), no research has investigated the intracellular ER stress-inducing effects of carbon quantum dots (CQDs) in ESC or ACS, presenting an avenue for further exploration.

Because there have been studies reporting that nitrogen doping of CQDs (NCQD) improves optical properties in biomedical applications (Dsouza et al. 2021), in this study we synthesized NCQDs and investigated their proliferation and differentiation effects using OG2 and MC3T3-E1 cells. Our investigation revealed that the toxicity of NCQDs is concentration-dependent, with low concentrations stimulating cell proliferation through the cell cycle activation. Furthermore, we verified the differentiation-inducing effect of NCQDs by examining the expression of fluorescent reporter in OG2 cells and various differentiation markers. To gain deeper insights into the mechanism, we also analyzed the expression of ER stress marker, establishing that NCQDs are involved in ER stress signaling pathways. Given the confirmed effects of NCQDs on cell cytotoxicity, proliferation and embryonic stem cell differentiation, we strongly advocate for comprehensive biosafety assessments before considering the widespread applications of NCQDs in living organisms. Understanding their

potential impacts on cellular processes and signaling pathways is crucial for responsible and safe utilization of these materials.

2. Materials and methods

2.1. Materials

Materials such as, DMEM (cat. No. LM001-05, Welgene) and alpha-MEM (cat. No. LM008-01; Welgene), FBS (cat. No. 30044-333, Gibco) and MEM NEAA (cat. No.11140-050, Gibco) and Glutamax (cat. No.35050-061, Gibco), 2-Mercaptoethanol (cat. no. 02194705, MP Biomedicals), penicillin-streptomycin (cat. No.15140-122, Gibco) and laduviglusib (glycogen synthase kinase 3 (GSK3) inhibitor (CHIR99021; cat. No. HY-10182, MCE)); mirdametinib (an inhibitor of mitogen activated protein kinase (MAPK)/ extracellular signal- regulated kinase (ERK) (PD0325901; cat. No.HY- 10254, MCE)), ESGRO® Recombinant Mouse LIF (cat. No. ESG1107), citric acid, urea, N, N-dimethylformamide (DMF), and hydrazine hydrate were purchased from Sigma-Aldrich. Ethyl alcohol, hydrochloric acid (HCl, 35.0–37.0%), sulfuric acid (H2SO4, 95%), and sodium hydroxide (NaOH, beads) were purchased from Samchun Chemical. Sigma-Aldrich) and DPBS (cat. No.LB001-02, Welgene, Korea), TRI-Reagent (cat. No. FATRR 001, FAVORGEN), AMPIGENE® cDNA Synthesis Kit (cat. No. ENZ-KIT106-0200, ENZO) and TOPreal™ qPCR 2X PreMIX (SYBR Green with low ROX; cat. No. RT500M; Enzynomics, Korea) and chloroform (cat. No. un1888, Duksan, Korea) and isopropyl alcohol (cat. No. un1219; Duksan; Korea), and effectene transfection reagent (cat. no. 301425, Qiagen) and gelatin (cat. no. 9000708, Duksan, Korea), pBOB-EF1-FastFUCCI-Puro vector (cat. 86849, Addgene), culture plates (96-well, 12-well, 6-well; SPL, Korea), and a Reagent Reservoir (cat. No. 95128095, Thermo Scientific™) and a D-Plus™ CCK cell viability assay kit (cat. No. CCK-3000, DonginLS, Korea), were purchased. A CO_2 incubator (Cat. No. NB-203XL, N-BIOTECH), an Inverted Laboratory Microscope Leica DM IL LED (Leica), and an ASTEC Thermal Cycler Gene Atlas (cat. No.HU, Astec), and Rotor-Gene Q 2plex (cat. No. 9001680, QIAGEN) and Epoch 2 Microplate Spectrophotometer (cat. No. EPOCH2NSC, Agilent Technologies) was used for all the experiments.

2.2. Synthesis of NCQD and characterization

NCQDs were prepared using the same molar ratios of urea and citric acid as precursors under microwave irradiation at 1000 W. Two mM of urea and 2 mM of citric acid were dispersed in 10 mL of DI water and graphitized in a microwave oven (MAS-II Plus, Sieno) at 180 °

C for 10 min. After the graphitization reactions, the NCQDs were collected by centrifugation at $10,000 \times g$ for 10 min to remove the solid aggregates, followed by dialysis with an MWCO 3.5 kDa membrane for 48 h to remove unreacted reactants. Finally, dark-brown NCQD powders were obtained by freeze drying for 48 h. UV absorption was measured using a Jasco V-670 UV-VIS-NIR spectrophotometer at the Future Energy Convergence Core Center (FECC). PL spectra were measured using a Jasco FP-6500 spectrofluorometer. High-resolution TEM images were obtained using a Tecnai G2 F20 transmission electron microscope at the Korea Institute of Science and Technology (KIST). X-ray photoelectron spectra (XPS) were measured by a NEXSA hybrid X-ray photoelectron spectrometer system at the Korea Basic Science Institute (KBSI). The FT-IR spectrum was obtained using Jasco FT/IR-4100 Infrared spectroscopy at the Future Energy Convergence Core center (FECC).

2.3. Cell culture and NCQD treatment

OG2 mouse ESCs were seeded into 0.5% gelatin-coated 96-well, 12-well, 6-well plates at densities of 5×10^3, 5×10^4 and 1×10^5 cells per well, respectively. The cells were cultured in DMEM media supplemented with 15% FBS, 1X Non-essential amino acid (NEAA), 1X Glutamax, 55 µM 2-Mercaptoethanol, 1X Penicillin-Streptomycin, 2i (3 µM CHIR99021 + 1 µM PD0325901), and 5×10^4 U/ ml LIF at 37 °C under 5% CO2 incubator. MC3T3-E1 cells were seeded into 96-well, 12-well, 6-well plates at a density of 5×10^3, 5×10^4, and 1×10^5 cells per well respectively alpha-MEM containing 10% FBS. Mouse embryonic fibroblast (MEF) were seeded into 6-well plates at a density of 1×10^5 cells per well in DMEM containing 10% FBS. Then, the culture medium containing NCQDs was treated at different concentrations (10, 20, 40, 80, 160 µg/ml). After 2–3 days, the NCQD treated cells were observed using an optical microscope. Additionally, to induce mild differentiation of OG2 cells, we treated the NCQD-containing medium without 2i reagents with OG2 cells for 3 days. The differentiation-inducing effect of the NCQDs was analyzed according to the intensity of the green fluorescence of OG2, and ImageJ software was used for quantitative analysis.

2.4. Cell viability and recovery in NCQD treatment

Cell viability was assessed using the D-Plus CCK Cell Viability Assay Kit. For the cell viability experiments with QD treatment, two types of cells at different stages, OG2

cells (1×10^4 cells) and MC3T3-E1 cells (5×10^3 cells) were seeded into individual 96-well plates with 100 µl of their respective complete media. After one day, a preliminary CCK assay was performed to ensure even cell seeding across all wells. In this preliminary assay, 10 µl of D-Plus™ CCK reagent was mixed with 90 µl of complete media and added to each well. The plate was briefly incubated to allow for the reaction, and the absorbance at 450 nm was measured using an Epoch 2 Microplate Spectrophotometer while maintaining a temperature of 37℃. Subsequently, all the CCK medium was removed, and the cells were washed with DPBS. Next, NCQDs were applied at verifying concentrations (5,10,20,40, and 80 µg/ml). After a 2-day incubation, the cells were treated with 5% CCK reagent, and cell viability was measured following the same procedure as described early. The measurements were independently repeated three times.

Wound healing assays were performed using MC3T3-E1 (1×10^5) cells MEF, and seeded in 6-well plates to assess cell proliferation and migration in response to different NCQD concentrations. When the cells reached approximately 80% confluence, a wound was created by gently scratching the center of the cell monolayer using a 1,000 µL-sized blue tip. Subsequently, the culture media were replaced with fresh culture media containing NCQDs at concentrations of 5, 10, 20, 40, 80, and 160 µg/ml. The progression of wound closure was observed daily, and images were captured using an optical microscope while maintaining a temperature of 37℃ and a 5% CO2 environment.

2.5. Fluorescence ubiquitin cell cycle indicator (FUCCI) analysis

HEK 293FT cell were seeded in 12-well plates at a density of 1×10^4 cells/well in complete growth medium. After 24 h, the pBOB-EF1-FastFUCCI-Puro vector was transfected using Effectene® Transfection Reagent according to the manufacturer's protocol. The ratio of DNA to enhancer was 1:8 and the ratio of DNA to Effectene was 1:25. The next day, NCQD (10,20 µg/ml) was treated in each FUCCI vector-transfected cell. Dual signals (green and red) were captured using a fluorescence microscope. Green and red fluorescence intensities were calculated independently.

2.6. qPCR analysis

Total RNA was isolated using TRI-Reagent following the manufacturer's instructions, after which reverse transcription was performed using an AMPIGENE® cDNA Synthesis Kit according to the manufacturer's manual.

Table 1. Real-time PCR primer sequences.

mGAPDH	forward	5′-AATGGTGAAGGTCGGTGTGAACGG-3′
	reverse	5′-GTCTCGCTCCTGGAAGATGGTGATG-3′
mOct4	forward	5′-CACCATCTGTCGCTTGGAGGC -3′
	reverse	5′-CTGCACCAGGGTCTCCGATTTG -3′
mNanog	forward	5′-CTTTCACCTATTAAGGTGCTTGC-3′
	reverse	5′-TGGCATCGGTTCATCATGGTA-3′
mSox2	forward	5′- CATGAGAGCAAGTACTGGCAAG-3′
	reverse	5′-CCAACGATATCAACCTGCATGG -3′
mGata4	forward	5′- CAGCAGCAGCAGTCAAGAGATG -3′
	reverse	5′- ACCAGGCTGTTCCAAGAGTCC -3′
mSox17	forward	5′-TTCTGTACACTTTAATGAGGCTGTTC-3′
	reverse	5′-TTGTGGGAAGTGGGATCAAG-3′
mBrachyury	forward	5′-ATCAGAGTCCTTTGCTAGGTAG-3′
	reverse	5′- GTTACAATCTTCTGGCTATGC-3′
mNestin	forward	5′-AACTGGCACACCTCAAGATGT-3′
	reverse	5′-TCAAGGGTATTAGGCAAGGGG-3′
mPax6	forward	5′- ACCAGTGTCTACCAGCCAATCC-3′
	reverse	5′- GCACGAGTATGAGGAGGTCTGA-3′
mPCNA	forward	5′- TTTGAGGCACGCCTGATCC -3′
	reverse	5′- GGAGACGTGAGACGAGTCCAT -3′
mCrebzf	forward	5′- CTGCCCGTCTTA ATCGGCTC-3′
	reverse	5′- CCGTAGGTAGCGACTCTCCTC-3′
mChop	forward	5′- CTGCAGTACCAAGTGGCACACT-3′
	reverse	5′- CCAGGACCTTCTGCTGAGTCTC′-3′
mATF6	forward	5′- TCGCCTTTTAGTCCGGTTCTT -3′
	reverse	5′- GGCTCCATAGGTCTGACTCC -3′

Quantitative PCR was performed using a TOP real™ qPCR 2X PreMIX and Rotor-Gene Q 2plex PCR machine. Each cDNA (100 ng/µl) was subjected to qPCR template. And the primer sequences are shown in Table 1. The qPCR was performed in Three-step with melt and the conditions were as follows; hold at 95℃ for 10 min, in cycle, denaturation at 95℃ for 30 s, annealing at annealing temperature for 60 s, extension at 72℃ for 60 s. Due to differences in the annealing temperature for each primer, the experiments were conducted separately (58℃-mSox2, mNanog, mSox17, mGata4, mBrachyury, mNestin, mPax6, 62℃-mOct4, mChop, touch down from 62℃ to 54℃- mPCNA, mATF6). mGAPDH was used as internal control to normalize the expression levels. The data were quantified using the $2^{-\triangle\triangle Ct}$ method.

2.7. Statistical analysis

The experimental data were presented on graphs as means ± the standard error of the mean (SEM). Statistical analysis was conducted using one-way analysis of variance (ANOVA), followed by a *t*-test performed using Microsoft Excel. Statistical significance was defined as $p < 0.05$.

3. Results

3.1. NCQD synthesis and characterization

NCQDs were successfully prepared under microwave irradiation using citric acid and urea as precursors at

the same molar ratio, as shown in Figure 1(A). The absorbance and photoluminescence (PL) of the NCQDs were investigated using a UV-vis spectrophotometer and spectrofluorometer, respectively. In Figure 1(B), the absorption peaks appeared at 260 and 335 nm of the NCQDs, which were attributed to the π-π* electronic transitions of C=C and C=N bonds from sp2-conjugations and the n-π* electronic transitions of C-O and C=O bonds, respectively (Maślana et al. 2020). The PL spectra of the NCQDs were recorded at 440 nm, and the excitation-dependent PL emissions of the NCQDs are shown in Figure 1(C), which highlights their highly ordered graphitic structures (Wang et al. 2020). NCQDs were characterized by high-resolution transmission electron microscopy (HRTEM). The size distribution ranging from 3 nm to 5 nm (Figure 1(D)). The inset of HRTEM image of NCQDs demonstrated their circular shapes of NCQDs with a visible crystalline lattice fringe, with a lattice spacing of 0.34 nm corresponding to the (0 0 2) facet of graphite (Song et al. 2019). X-ray photoelectron spectroscopy (XPS) and Fourier transform infrared spectroscopy (FT-IR) were employed to analyze the elemental composition and surface functional groups of NCQDs. In Figure 1(E), the XPS survey spectrum showed three distinctive peaks at 284.4, 399.4, and 532.0 eV for C1s, N1s, and O1s, respectively. The high resolution XPS spectrum of C1s have three binding energy peaks at 284.6, 285.9, and 287.5 eV to be assigned to the C-C/C=C, C-N/C-O, and C=O bonds, which are attributed to the doped nitrogen in the core of NCQDs and oxygen-
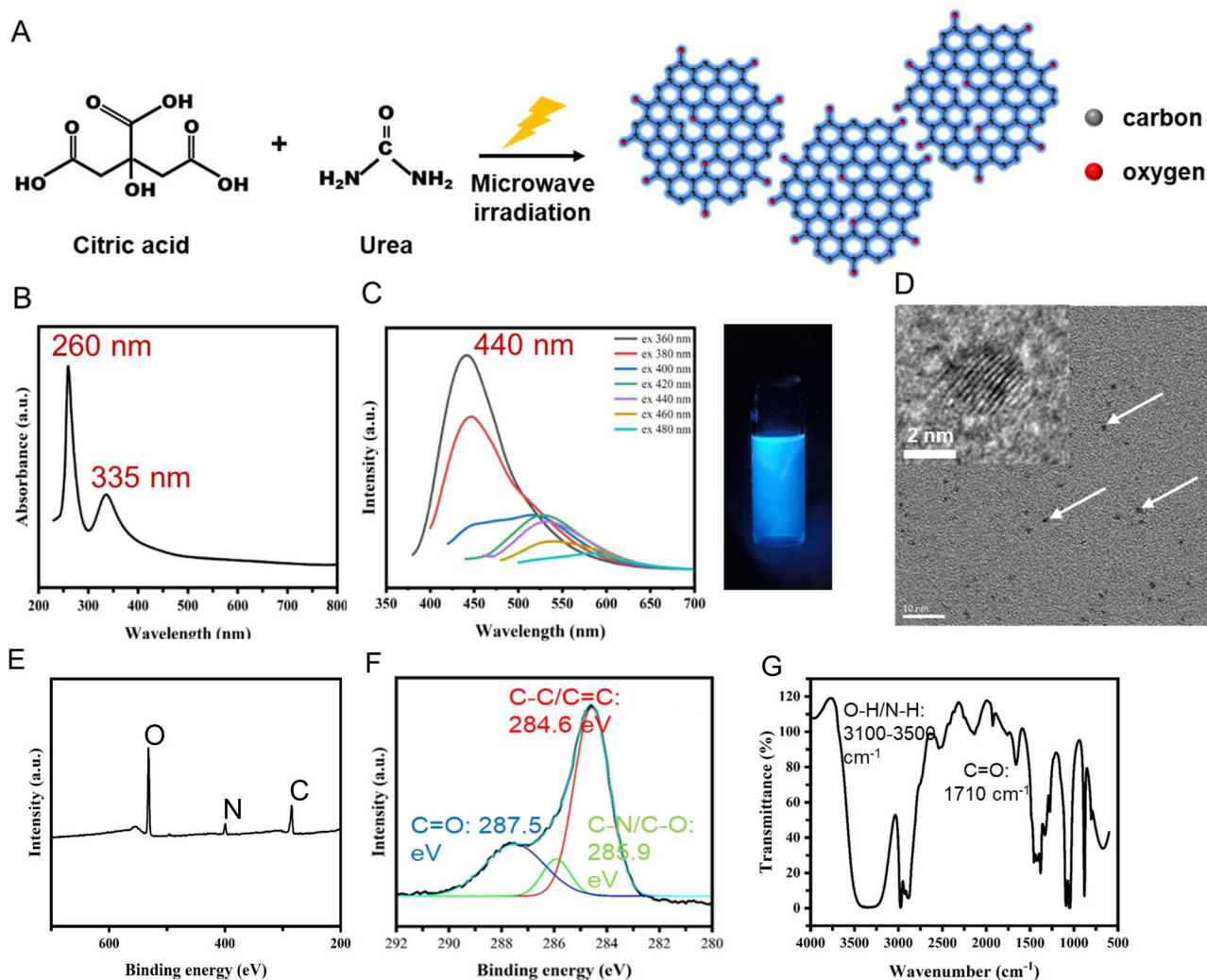

Figure 1. **Characterization of NCQDs**. A schematic presentation of NCQD Production. (B) absorption of NCQDs by UV-vis. (C) fluorescence spectrum of NCQDs under different wavelengths of excitation (360nm–480 nm), and suspension of NCQDs in DW under UV irradiation at 365 nm. (D) Representative HRTEM image of NCQDs. White arrows indicate NCQDs. (E) X-ray photoelectron spectroscopy (XPS) survey spectrum of NCQDs. The three distinctive peaks indicate oxygen, nitrogen, and carbon. (F) High-resolution XPS spectrum of C1s indicates three binding energy peaks as C-C/C=C, C-N/C-O, and C=O in the core of NCQDs. (G) FT-IR spectrum of NCQDs indicate absorption bands of ν(O-H), ν(N-H), and ν(C=O).

included functional groups on the NCQDs' surface (Figure 1(F)). In addition, FT-IR spectrum of NCQDs showed v(O-H) and v(N-H) in hydroxyl and amine groups at the range of 3100–3500 cm^{-1}, v(C = O) in carboxyl groups at the absorption band of 1710 cm^{-1} (Figure 1(G)).

3.2. Cell proliferation and cytotoxicity by NCQDs

A CCK assay was performed using OG2 and MC3T3-E1 cells treated with various concentrations of NCQDs to determine the effect of NCQD on cell viability. We confirmed that the proliferation of both types of cells was significantly improved at a concentration of 10 μg/ml NCQD, and that cell proliferation was commonly inhibited at concentrations above 30 μg/ml (Figure 2(A and B)). To determine whether the enhancement of cell proliferation by low-concentration NCQDs and the

inhibition of high-concentration NCQDs were related to the cell cycle, the expression of proliferating cell nuclear antigen (PCNA) was examined in OG2 cells using QPCR analysis. The results show that the expression of PCNA is significantly enhanced at a concentration of 10 ug/ml and rapidly decreases above the concentration of 40 ug/ml (Figure 2(C)). Upon inspecting OG2 cell colonies, we observed an increase in colony size at a concentration of 10 μg/ml of NCQD. However, both the size and number of colonies decreased compared to the control group at concentrations of 40 μg/ml or higher. Furthermore, at a concentration of 160 μg/ml of NCQD, the majority of OG2 cells were observed to have perished. (Figure 2(D)). In MC3T3-E1 cells, a type of ASCs, distinct differences were noted in the cell proliferation effect corresponding to the treatment with various NCQD concentrations. We treated MC3T3-E1 osteoblastic progenitor cells and MEF that
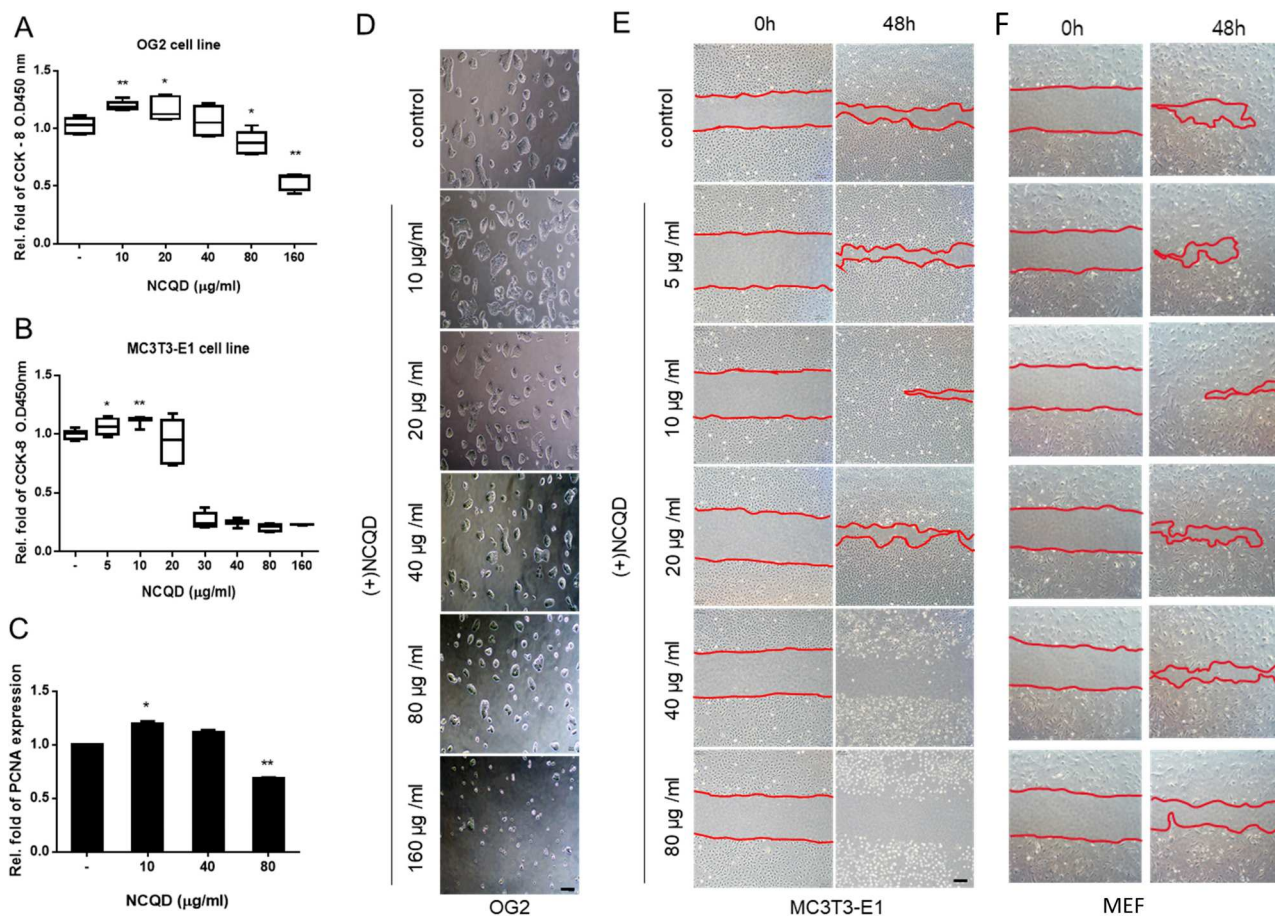

Figure 2. NCQDs affect cell viability and proliferation. A–B CCK-8 analysis results after 48 h of treatment with OG2(A) and MC3T3-E1 cells (B) with NCQDs at various concentrations (10–160) ug/ml; (C) OG2 treated with NCQD at different concentrations for 3 days, and proliferation effects were assessed by comparing PCNA mRNA expression level using q-RT PCR. The graphs of each fold change were drawn using Prism 6 (GraphPad Software). Data was normalized to control and presented as mean ± SEM of N = 3 experiments. (*$p < 0.05$, **$p < 0.01$, compared with non-NCQD treated group). (D) Morphology of OG2 cell treated with NCQD by concentration. Scale bar = 20 μm. (E–F) Wound-healing assay after treatment with each concentration of NCQDs into MC3T3-E1 cells and mouse embryonic fibroblast. The boundaries of each wound were indicated in red line. Scale bar = 200 μm

play roles in recovery through cell proliferation and differentiation in wound or damaged tissues with NCQDs at different concentrations and performed a Wound Healing Assay. As cell migration progressed, wound closure was more pronounced in the 10 and 20 µg/ml of NCQD treatment groups compared to the control. Especially, it was most densely filled at 10 µg/ml and showed a lot of proliferation, which is consistent with the CCK results. Cell death was observed starting at 40 µg/ml NCQD, and most cells died at a concentration of 80 µg/ml (Figure 2(E–F)). In summary, this figure shows that NCQD at a concentration of 10 µg/ml has the effect of significantly improving the proliferation of OG2, MC3T3-E1, and MEF cells and that concentrations above 30 µg/ml inhibit proliferation or induce death depending on the cell type.

3.3. Cell cycle activation by NCQDs

HEK293FT cells were transfected with a fluorescent ubiquitin cell cycle indicator (fucci) system vector (Figure 3(A)) to confirm whether the cell proliferation effect of NCQDs induces cell cycle activation. We further analyzed the change in fluorescence after treatment with NCQDs at concentrations of 10 and 20 µg/ml. In the control group, most cells showed red fluorescence in the G1 phase; however, but in the NCQD-treated group, the number of cells entering the S/G2/M phase and showing green fluorescence dramatically increased (Figure 3(B and C)). These results indicate that NCQDs induce cell proliferation by activating the cell cycle.

3.4. The effect of NCQD on ESC differentiation

To determine whether NCQDs also affect the pluripotency of embryonic stem cells, we observed cell responses after treating OG2 cells with various concentrations of NCQDs. Mild differentiation induction and NCQD treatment at various concentrations for 3 days in OG2 cells using culture medium without 2i confirmed that the GFP intensity rapidly decreased in a concentration-dependent manner in the NCQD-treated group (Figure 4(A)). In addition, the observation of morphological differences between the undifferentiated and induced groups showed that the fibers of the cells in the differentiation group became longer. In particular, it can be seen that above 20 µg/ml, round cell colonies were broken and rapid decrease in GFP, indicating differentiation (Figure 4(A)). We also analyzed and graphed the GFP intensity changes (Figure 4(B)). Taken together, these results confirm that NCQDs suppress the pluripotency of embryonic stem cells by inhibiting the activity of OCT4-enhancer. Next, to confirm the effect of

NCQDs on the induction of embryonic stem cell differentiation, we analyzed the expression of pluripotency and differentiation marker genes using qPCR. In the differentiation-induced group, the expression of pluripotency markers, Oct4, Nanog, and Sox2 was significantly reduced compared to that in control group (Figure 5(A–C)). Additionally, a significant difference was evident based on the concentration of the NCQDs. At 10 µg/ml, there was a slight increase in the expression of pluripotency markers, while there was a significant decrease in the 80 µg/ml group. (Figure 5(A–C)). The expression of differentiation markers was also significantly increased in the group which differentiation was normally induced. The expression of the endoderm marker Gata4 and the mesoderm markers sox17 and Brachyury were significantly increased at a concentration of 80 ug/ml NCQD, but interestingly, the expression of the ectoderm marker, Nestin, and Pax6, was significantly decreased at a concentration of 80 ug/ml NCQD (Figure 5(D–H)). We confirmed that 10 µg/ml of NCQDs had an inhibitory effect on the differentiation of embryonic stem cells, but that 80 µg/ml accelerated differentiation, and in particular, induced differentiation into endoderm and mesoderm cell lineages.

3.5. ER stress by NCQD

We examined the expression of the ER stress markers Crebzf, Chop and ATF6 to determine whether ER stress is involved in the cellular response to NCQD treatment. When OG2 differentiation was induced, the expression of the Crebzf gene significantly increased. The group treated with NCQDs at a concentration of 40 ug/ml or more showed relatively stronger Crebzf gene expression (Figure 6(A)). Regarding the Chop gene, we observed no alteration in expression level attributable to the differentiation of OG2 cells. However, intriguingly, at concentrations exceeding 40 µg/ml of NCQD, we noted a notably stronger expression level. (Figure 6(B)). In contrast, the expression level of ATF6 significantly decreased when the differentiation of OG2 cells was induced, and no difference was observed depending on the concentration of NCQD (Figure 6(C)). These results show that high concentrations of NCQDs induce the abnormal differentiation of OG2 cells by stimulating the ER stress signaling mechanism mediated by Chop and Crebzf.

4. Discussion

QDs based on heavy metals like cadmium exhibit a narrow full-width half-maximum of approximately 30 nm, a size-controllable band gap, and high quantum yield (>90%), albeit with significant biotoxicity
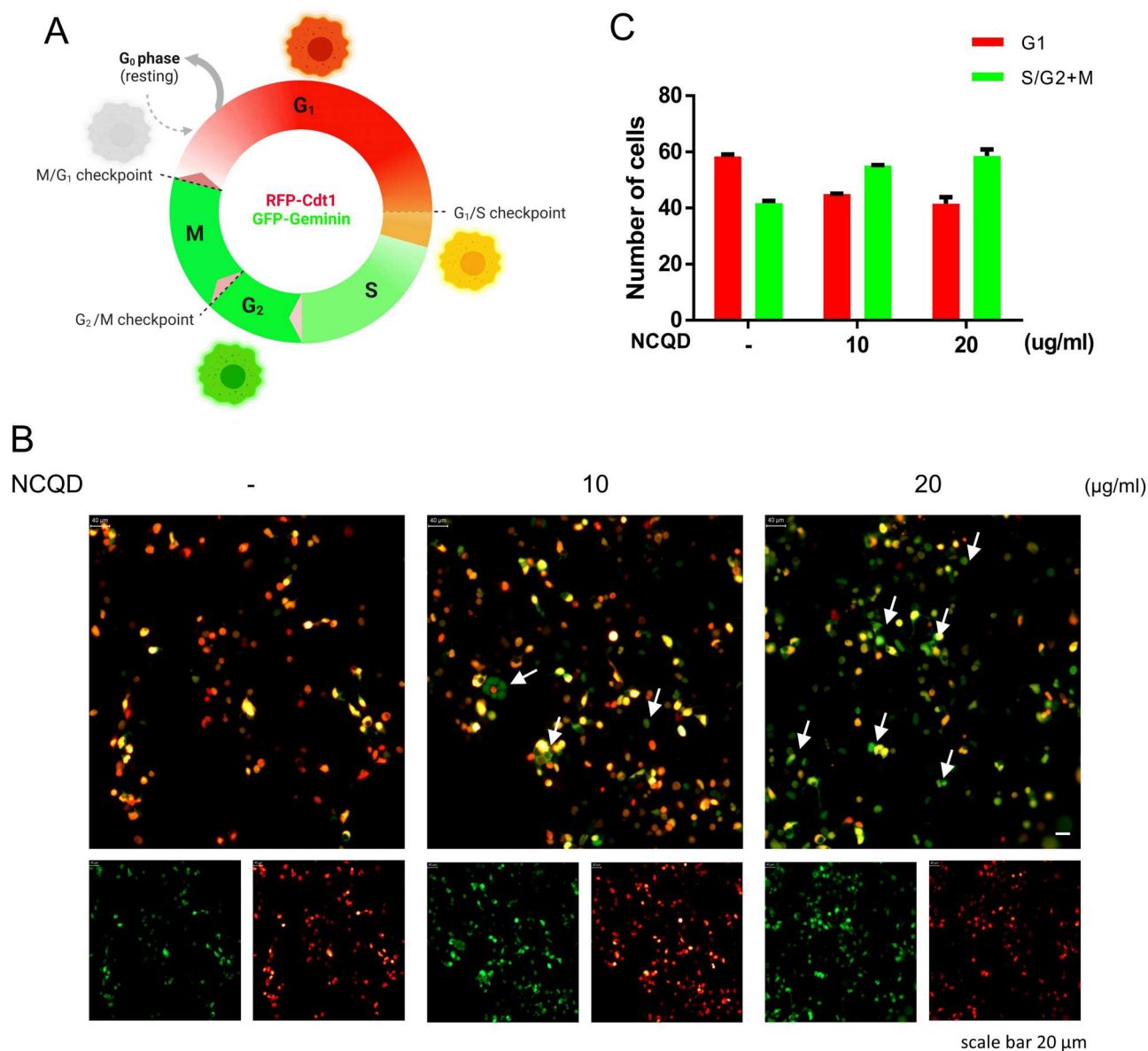
Figure 3. NCQD promotes proliferation by activating cell cycle. (A) Schematic diagram of FUCCI system. Cells in G1 phase express RFP through the cdt promoter, and cells in S/G2/M phase express GFP through the geminin promoter. (B) FUCCI-trasnfected HEK29FT cells were treated with NCQD at each concentration (-, 10, 20 µg/ml). 3days after NCQD treatment, cells were observed under a fluorescence microscope. Scale bar = 40 µM (C)**.** The graph depicted values obtained by dividing cells expressing either GFP or RFP alone by the total cell count. The graphs of each fold change were drawn using Prism 6 (GraphPad Software). Data was normalized to control and presented as mean ± SEM of N = 3 experiments.

(Haque et al. 2013; Shen et al. 2019; Chen et al. 2021). However, carbon-based QDs (CQDs) have relatively low biotoxicity and have various applications, including electronic and optoelectronic devices (Zhang et al. 2020). CQDs are located inside cells through endocytosis and exhibit fluorescence; therefore, have been widely studied as biomarkers for cell imaging (Lim et al. 2015). These cell imaging technologies play a key role in understanding the internal structure and function of cells. CQDs synthesized with adjustable sizes can further increase the luminous efficiency owing to the improvement in optoelectronic properties through continuous modification (Frecker et al. 2015). Numerous researchers are investigating biocompatibility factors like lower toxicity and intracellular stability to advance the efficiency of cell imaging using CQDs. Similarly, our focus has been on exploring biocompatible CQD synthesis methods, including NCQDs. In this study, we explored the effects of our synthesized NCQDs on cytotoxicity and various cellular responses, to bridge the gap between in vivo and in vitro studies of future QDs and their applications in the biomedical life sciences.
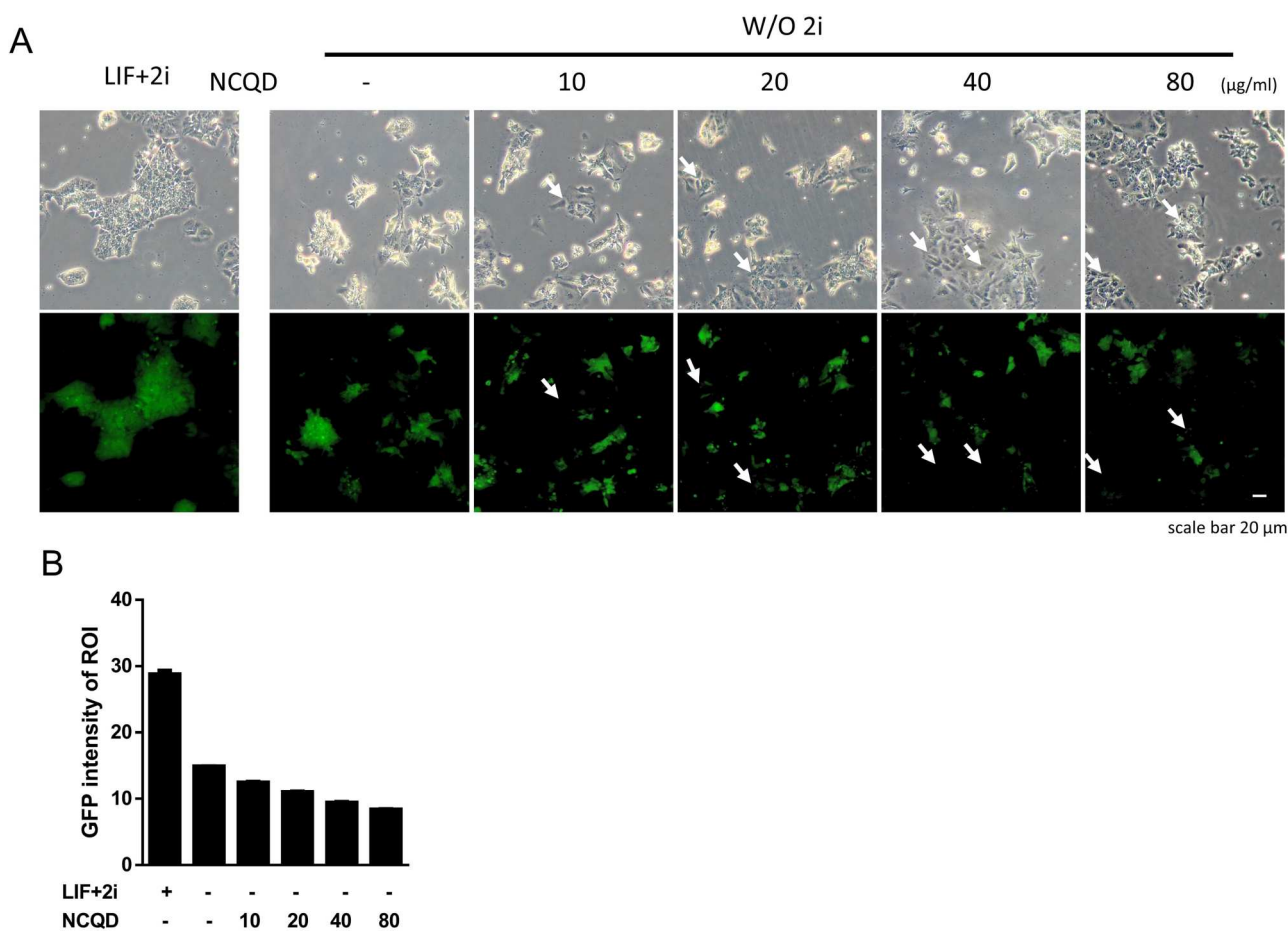
Figure 4. NCQDs induce differentiation of mESC. (A) OG2 mESC were seeded and maintained on 2i free media to confirm the differentiation on NCQD. Treated with NCQD at varying concentrations, followed by observation under fluorescence microscopy after 3 days. White arrows indicate cell differentiation, disappeared of GFP. Scale bar = 20 μm. (B) The graph shows the measured GFP intensity through ROI in each image. The graph was drawn using Prism 6 (GraphPad Software). Values presented as mean ± SEM of N = 2 experiments.

Toxicity studies using various types of QDs have been conducted on various species. Animal cell culture experiments have shown that cadmium-based QDs transferred to the cell cytoplasm, released free cadmium, and produced free radical species, which can lead to strong toxicity (Tsoi et al. 2013). Given the perceived high risk associated with metal-based quantum dots (QD) for use in the human body, the choice of carbon-based QDs becomes imperative for biomedical applications. A study employing algae conducted comparative toxicity assessment between carbon-based QDs (CQDs) and metal-based QD (MQDs), with findings indicating lower toxicity of CQDs compared to MQDs. However, it's worth noting that the toxicity profile may vary depending on the specific type of MQDs, with some reported to exhibit lower toxicity than CQDs (Xiao et al. 2016). However, animal experiments have shown different trends. When QDs are injected intravascularly, they primarily travel to the liver and spleen, and if their diameter is larger than 6 nm, they

are excreted; therefore, they appear to be relatively safe in animals. Because extensive studies on the toxicity of different types of modified QDs in cells and animals are needed, we performed cell experiments using NCQDs produced using a rapid microwave synthesis method. We expected NCQDs to be less toxic, and because each stem cell type, such as embryonic stem cells and adult stem cells, has unique characteristics and potential, we performed CCK analysis using OG2 and MC3T3-E1 cells. However, the cytotoxicity of the NCQDs in the two cell types was different. In the case of OG2, a decrease in proliferation began at 80 μg/ml and showed apoptosis at a concentration of 160 μg/ml (Figure 2(D)), while in the case of MC3T3-E1, rapid cell death occurred at 40 μg/ml (Figure 2(E)). Thus, it can be inferred that the application of QDs to living organisms requires careful concentration adjustments based on sufficient prior research.

Interestingly, when treated with a low concentration of NCQD, approximately 10 ug/ml, both types of cells
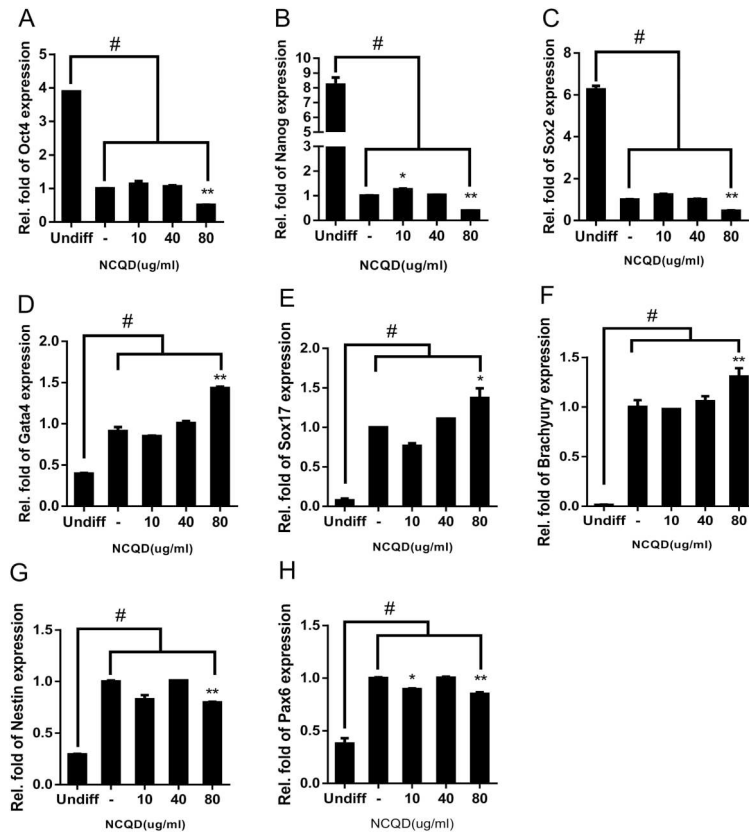
Figure 5. Identification differentiation induced by NCQD. OG2 seeded without 2i was treated with NCQD at different concentrations for 3days, and their cDNA was prepared to compare relative mRNA expression. Expression level of pluripotency (A–C) and differentiation marker (D–H) were analyzed by q-RT PCR. The graphs of each fold change were drawn using Prism 6 (GraphPad Software). Data was normalized to control and presented as mean ± SEM of N = 3 experiments. (*$p < 0.05$, **$p < 0.01$, compared with non-NCQD treated group, #$p < 0.01$ compared with undifferentiated ES cells).

showed a significant cell proliferation. Additionally, we confirmed that PCNA, a protein that plays a key role in the cell cycle, was deeply involved in the regulation of cell proliferation by NCQDs (Figure 2(C)). Existing studies have primarily focused on comparing quantum dot (QD) and proliferating cell nuclear antigen (PCNA) immunostaining as bioimaging markers. However, there has been no investigation into the impact of QDs
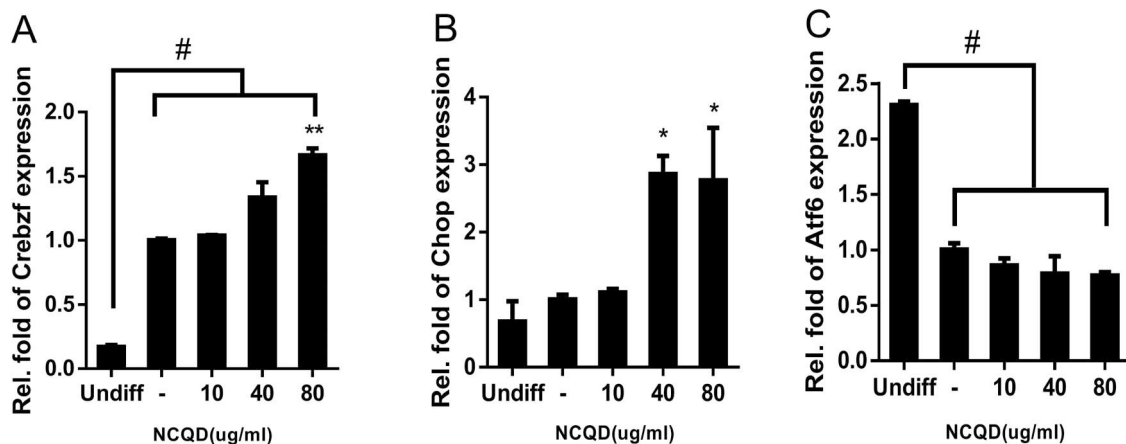
Figure 6. Analysis of ER stress in response to NCQD treatment. To comprehend differentiation induced by NCQD, expression of representative ER stress marker, Crebzf, Chop, ATF6 (A–C) was examined. The graphs of each fold change were drawn by Prism 6 (GraphPad Software). Data was normalized to control and presented as mean ± SEM of N = 3 experiments. (*$p < 0.05$, **$p < 0.01$, compared with non-NCQD treated group, #$p < 0.01$ compared with undifferentiated ES cells).

on PCNA expression. Consequently, we are conducting additional mechanistic studies to explore the hypothesis that NCQDs influence entry into the S phase of the cell cycle by modulating PCNA activity. One of our supplementary experiments involved a cell cycle reporting assay utilizing the Fucci system. To examine the growth of cell proliferation from a cell cycle perspective, the FUCCI (Fluorescence ubiquitin cell cycle indicator) system, is a useful tool that can monitor the cell cycle by imaging in living cells. The cells to which the Fucci system was applied exhibited different fluorescence colors depending on the cell cycle (Figure 3(A)). The G1 cell-specific cdt1 promoter expresses a red fluorescent gene, and the S/G2/M cell-specific geminin promoter expresses a green fluorescent gene (Zielke and Edgar 2015). We examined the cell cycle rate by transfecting HEK293FT cells with the FUCCI system vector and then treating them with NCQDs (Figure 3(B)).

Evaluating the effect of NCQDs on embryonic stem cells requires not only the evaluation of cell growth but also differentiation studies. The OG2 cell line is an embryonic stem cell line with a GFP gene applied to the enhancer of Oct4, a pluripotency marker, and the progress of ESC differentiation can be quickly and easily confirmed using fluorescence microscopy (Do and Scholer 2010). We observed changes in the cell colonies and shapes when OG2 cells were treated with high concentrations of NCQDs. We verified that this phenomenon resembles the induction of ESC differentiation, leading to the disappearance of GFP in OG2 cells. Consequently, we examined the expression of pluripotency markers and markers for the three germ layers in OG2 cells treated with varying concentrations of NCQDs. Furthermore, to ensure a more definitive effect, we induced mild differentiation by employing a medium without GSK3β and ERK/MEK inhibitor (2i), a strong factor for pluripotency maintenance.

As anticipated, NCQDs significantly induced the differentiation of OG2 cells. They downregulated the expression of representative pluripotency markers
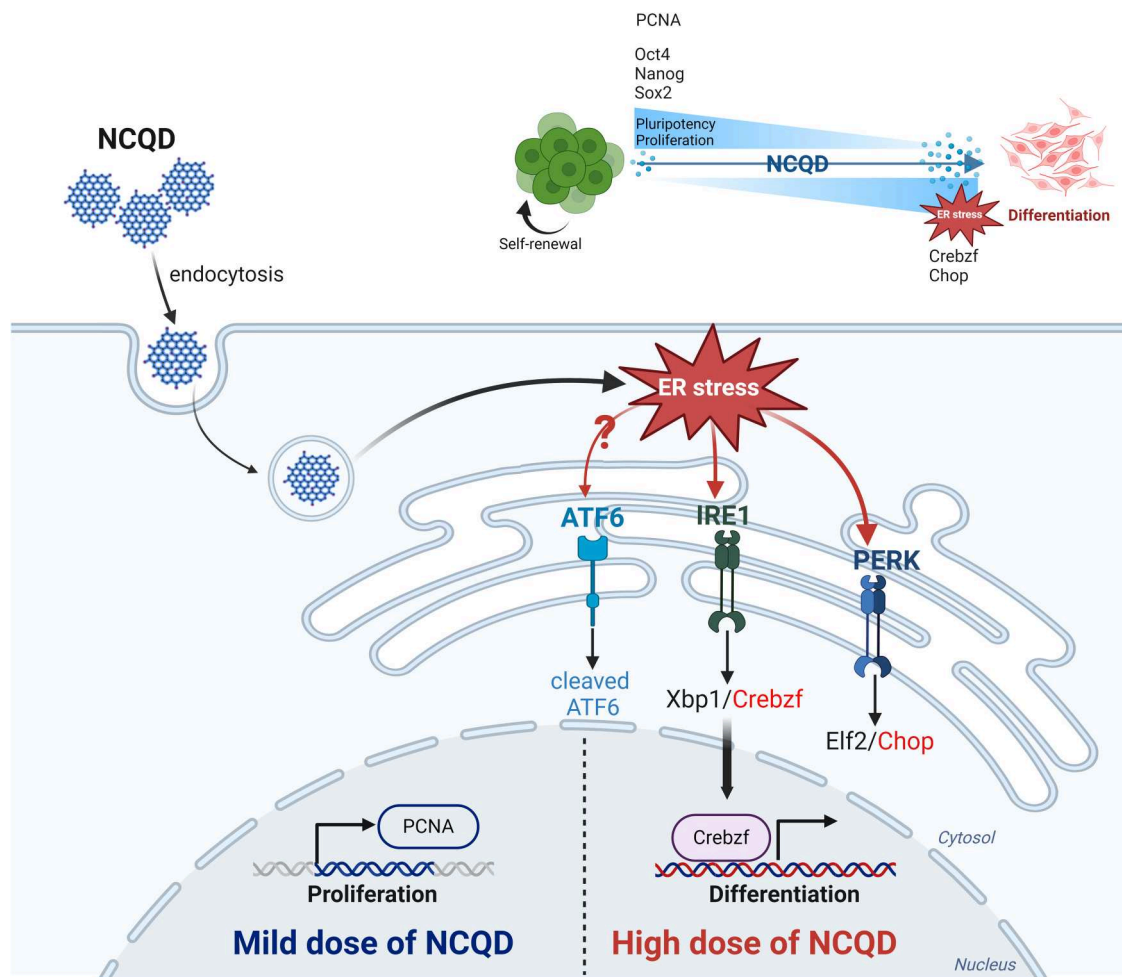

Figure 7. Model of the effect of NCQDs in animal cells. NCQDs transferred into cells by endocytosis may cause ER stress through the IRE1 and PERK signaling pathways of the ER membrane. Depending on the concentration of NCQDs, the effect of inducing ER stress increases and reduces the pluripotency of ESCs, leading to unspecific differentiation.

Oct4, Sox2, and Nanog, while concurrently upregulating the expression of Gata4, Sox17, and Brachyury. However, a recent study reported controversial findings, suggesting that graphene-based QDs inhibit differentiation by suppressing methylation in the Sox2 promoter (Ku et al. 2021). We investigated this discrepancy and concluded that it stemmed from differences in the QDs utilized in both studies. Given these conflicting results, we advocate for future research encompassing various types of synthesized QDs. Interestingly, our study confirmed that NCQDs induced the expression of endodermal and mesodermal marker genes, but reduced that of ectodermal marker genes. We plan to conduct further studies to validate these results.

ER stress arises when critical biological processes like the unfolded protein response (UPR) undergo alterations, impacting gene expression regulation and various cell survival including immune cells (Lee et al. 2019; Gao et al. 2024). We postulated that NCQDs contribute to the induction of OG2 cell differentiation by escalating ER stress. Consequently, we scrutinized the expression levels of representative ER stress markers including Crebzf, Chop and ATF6. The CHOP protein serves as hallmark in the PERK signaling mechanism (Rozpedek et al. 2016), while Crebzf is linked with xbp1, a component of the Ire1 signaling pathway (Potapov et al. 2015). Our findings revealed notable insights. Upon induction of cell differentiation, ER stress-mediated UPR signaling via Crebzf surged rapidly, whereas ATF6 signaling showed a significant decline. Interestingly, chop seemed unrelated to the differentiation induction process. Moreover, the impacts of NCQDs on ER stress markers varied across the three types of markers. NCQDs substantially boosted the expression of Crebzf and Chop but exhibited no effect on ATF6 expression. Further exploration of the chaperone activity, a downstream event in ATF6 signaling, is required to verify the influence of NCQD on ATF6 signaling. Our results imply that NCQDs are pivotal in PERK signaling. Although ER stress studies on QDs are abundant, most focus on MQDs, with no prior reports on ER stress in NCQDs. Consequently, we suggest that among the three UPR signaling mechanisms, NCQDs predominantly affect PERK/eIF2a/CHOP signaling while ATF6 remains unaffected (Figure 7).

5. Conclusion

This study aimed to comprehensively investigate the influence of QDs on cellular proliferation, aiming to provide valuable insights into their biological interactions. The findings are expected to contribute to the effective utilization of QDs in various biomedical applications while safeguarding cellular proliferation and overall biological functionality. Furthermore, it is suggested that these insights may extend beyond cellular behavior and potentially impact the in vivo stages of embryonic development. To gain a deeper understanding, further research is warranted to elucidate the mechanisms underlying NCQD-induced cell proliferation and ER stress. Additionally, in vivo investigations are essential to assess the potential side effects of high doses of NCQDs on embryos and reproduction. These endeavors will be crucial in advancing our knowledge of the broader implication of QDs in biological systems. NCQDs exhibit toxicity to ESCs and ASCs above a specific concentration threshold, leading to abnormal differentiation of ESCs into ectodermal and mesodermal cells. Interestingly, NCQDs enhance cell proliferation and sustain cell pluripotency at low concentrations. These effects of NCQDs seem intricately linked to the intracellular ER stress signaling mechanism. Hence, we propose that further diversified research into the biomedical application of NCQDs is imperative for the future.

Author contributions

Hyunhee Song performed the experiments and wrote the manuscript. Hyunwoo Choi provided the OG2 cells and discussed of OG2 differentiation. Seonghan Kim synthesized the NCQDs. Sangmin An provided the equipment and discussed the experiments. Hwan Gyu Kim provided additional equipment and discussion for revision. Sejung Kim oversaw the NCQD synthesis and discussed the direction of the research. Hoon Jang supervised all the study and wrote the manuscript.

ORCID

Hoon Jang http://orcid.org/0000-0001-8875-6854

References

Adachi Y, Yamamoto K, Okada T, Yoshida H, Harada A, Mori K. 2008. ATF6 is a transcription factor specializing in the regulation of quality control proteins in the endoplasmic reticulum. Cell Struct Funct. 33:75–89. doi:10.1247/csf.07044.

Akhavan O, Ghaderi E, Akhavan A. 2012. Size-dependent genotoxicity of graphene nanoplatelets in human stem cells. Biomaterials. 33:8017–8025. doi:10.1016/j.biomaterials.2012.07.040.

Bai C, Yao Y, Wang Z, Huang X, Wei T, Zou L, Liu N, Zhang T, Tang M. 2022. CdTe quantum dots trigger oxidative stress and endoplasmic reticulum stress-induced apoptosis and autophagy in rat Schwann cell line RSC96. J Appl Toxicol. 42:1962–1977. doi:10.1002/jat.4367.

Banerjee S, Wong SS. 2003. In situ quantum dot growth on multiwalled carbon nanotubes. J Am Chem Soc. Aug 27;125:10342–10350. doi:10.1021/ja035980c.

Blanco-Gelaz MA, Suarez-Alvarez B, Ligero G, Sanchez L, Vidal-Castiñeira JR, Coto E, Moore H, Menendez P, Lopez-Larrea C. 2010. Endoplasmic reticulum stress signals in defined human embryonic stem cell lines and culture conditions. Stem Cell Rev Rep. 6:462–472. doi:10.1007/s12015-010-9135-4.

Boiani M, Eckardt S, Schöler HR, McLaughlin KJ. 2002. Oct4 distribution and level in mouse clones: consequences for pluripotency. Genes Dev. 16:1209–1219. doi:10.1101/gad.966002.

Caballano-Infantes E, Terron-Bautista J, Beltran-Povea A, Cahuana GM, Soria B, Nabil H, Bedoya FJ, Tejedo JR. 2017. Regulation of mitochondrial function and endoplasmic reticulum stress by nitric oxide in pluripotent stem cells. World J Stem Cells. Feb 26;9:26–36. doi:10.4252/wjsc.v9.i2.26.

Cao SS, Kaufman RJ. 2012. Unfolded protein response. Curr Biol. 22:R622–R626. doi:10.1016/j.cub.2012.02.021.

Chakrabarti A, Chen AW, Varner JD. 2011. A review of the mammalian unfolded protein response. Biotechnol Bioeng. 108:2777–2793. doi:10.1002/bit.23282.

Chen J, Wang J, Xu X, Li J, Song J, Lan S, Liu S, Cai B, Han B, Precht JT, et al. 2021. Efficient and bright white light-emitting diodes based on single-layer heterophase halide perovskites. Nat Photonics. 15:238–244. doi:10.1038/s41566-020-00743-1.

Chen M-L, He Y-J, Chen X-W, Wang J-H. 2013. Quantum-dot-conjugated graphene as a probe for simultaneous cancer-targeted fluorescent imaging, tracking, and monitoring drug delivery. Bioconjugate Chem. 24:387–397. doi:10.1021/bc3004809.

Chong Y, Ma Y, Shen H, Tu X, Zhou X, Xu J, Dai J, Fan S, Zhang Z. 2014. The in vitro and in vivo toxicity of graphene quantum dots. Biomaterials. 35:5041–5048. doi:10.1016/j.biomaterials.2014.03.021.

Do JT, Scholer HR. 2010. Cell fusion-induced reprogramming. Methods Mol Biol. 636:179–190. doi:10.1007/978-1-60761-691-7_11.

Dong Y, Li G, Zhou N, Wang R, Chi Y, Chen G. 2012. Graphene quantum dot as a green and facile sensor for free chlorine in drinking water. Anal Chem. 84:8378–8382. doi:10.1021/ac301945z.

Dsouza SD, Buerkle M, Brunet P, Maddi C, Padmanaban DB, Morelli A, Payam AF, Maguire P, Mariotti D, Svrcek V. 2021. The importance of surface states in N-doped carbon quantum dots. Carbon NY. 183:1–11. doi:10.1016/j.carbon.2021.06.088.

Frecker T, Bailey D, Arzeta-Ferrer X, McBride J, Rosenthal SJ. 2015. Quantum dots and their application in lighting, displays, and biology. ECS J Solid State Sci Technol. 5:R3019. doi:10.1149/2.0031601jss.

Gao Y, Ryu H, Lee H, Kim YJ, Lee JH, Lee J. 2024. ER stress and unfolded protein response (UPR) signaling modulate GLP-1 receptor signaling in the pancreatic islets. Mol Cells. Jan;47:100004. Epub 20231215. doi:10.1016/j.mocell.2023.12.002.

Haque MM, Im HY, Seo JE, Hasan M, Woo K, Kwon OS. 2013. Acute toxicity and tissue distribution of CdSe/CdS-MPA quantum dots after repeated intraperitoneal injection to mice. J Appl Toxicol. 33:940–950. doi:10.1002/jat.2775.

Hsieh M-S, Shiao N-H, Chan W-H. 2009. Cytotoxic effects of CdSe quantum dots on maturation of mouse oocytes, fertilization, and fetal development. Int J Mol Sci. 10:2122–2135. doi:10.3390/ijms10052122.

Huang N, Cheng S, Zhang X, Tian Q, Pi J, Tang J, Huang Q, Wang F, Chen J, Xie Z. 2017. Efficacy of NGR peptide-modified PEGylated quantum dots for crossing the blood–brain barrier and targeted fluorescence imaging of glioma and tumor vasculature. Nanomedicine: Nanotechnology. Biol Med. 13:83–93.

Jang H, Kim E-J, Park J-K, Kim D-E, Kim H-J, Sun W-S, Hwang S, Oh K-B, Koh J-T, Jang W-G, Lee J-W. 2014. SMILE inhibits BMP-2-induced expression of osteocalcin by suppressing the activity of the RUNX2 transcription factor in MC3T3E1 cells. Bone. 61:10–18. doi:10.1016/j.bone.2013.12.028.

Ji Y, Kim J, Cha A-N, Lee S-A, Lee MW, Suh JS, Bae S, Moon BJ, Lee SH, Lee DS, et al. 2016. Graphene quantum dots as a highly efficient solution-processed charge trapping medium for organic nano-floating gate memory. Nanotechnology. 27:145204. doi:10.1088/0957-4484/27/14/145204.

Kamrani S, Rezaei M, Kord M, Baalousha M. 2018. Transport and retention of carbon dots (CDs) in saturated and unsaturated porous media: role of ionic strength, pH, and collector grain size. Water Res. 133:338–347. doi:10.1016/j.watres.2017.08.045.

Kim H-I, Moon S-H, Lee W-C, Lee H-J, Shivakumar SB, Lee S-H, Park B-W, Rho G-J, Jeon B-G. 2018. Inhibition of cell growth by cellular differentiation into adipocyte-like cells in dexamethasone sensitive cancer cell lines. Animal Cells Syst (Seoul). 22:178–188. doi:10.1080/19768354.2018.1476408.

Kratochvilova K, Moran L, Padourova S, Stejskal S, Tesarova L, Simara P, Hampl A, Koutna I, Vanhara P. 2016. The role of the endoplasmic reticulum stress in stemness, pluripotency and development. Eur J Cell Biol. Mar–May;95:115–123. Epub 20160206. doi:10.1016/j.ejcb.2016.02.002.

Ku T, Hao F, Yang X, Rao Z, Liu QS, Sang N, Faiola F, Zhou Q, Jiang G. 2021. Graphene quantum dots disrupt embryonic stem cell differentiation by interfering with the methylation level of Sox 2. Environ Sci Technol. 55:3144–3155. doi:10.1021/acs.est.0c07359.

Kurosawa S, Hashimoto E, Ukai W, Toki S, Saito S, Saito T. 2007. Olanzapine potentiates neuronal survival and neural stem cell differentiation: regulation of endoplasmic reticulum stress response proteins. J Neural Transm. 114:1121–1128. doi:10.1007/s00702-007-0747-z.

Kwon J, Kim J, Kim KI. 2023. Crosstalk between endoplasmic reticulum stress response and autophagy in human diseases. Animal Cells Syst (Seoul). 27:29–37. Epub 20230223. doi:10.1080/19768354.2023.2181217.

Lee SW, Park HJ, Kim SH, Shin S, Kim KH, Park SJ, Hong S, Jeon SH. 2019. TLR4-dependent effects of ISAg treatment on conventional T cell polarization in vivo. Animal Cells Syst (Seoul). Jun;23:184–191. Epub 20190425. doi:10.1080/19768354.2019.1610059.

Lee Y, Kwon J, Jeong JH, Ryu JH, Kim KI. 2022. Kazinol C from Broussonetia kazinoki stimulates autophagy via endoplasmic reticulum stress-mediated signaling. Animal Cells Syst (Seoul). 26:28–36. Epub 20220110. doi:10.1080/19768354.2021.2023628.

Lim SY, Shen W, Gao Z. 2015. Carbon quantum dots and their applications. Chem Soc Rev. 44:362–381. doi:10.1039/C4CS00269E.

Mansuriya BD, Altintas Z. 2020. Applications of graphene quantum dots in biomedical sensors. Sensors. 20:1072. doi:10.3390/s20041072.

Maślana K, Kaleńczuk RJ, Zielińska B, Mijowska E. 2020. Synthesis and characterization of nitrogen-doped carbon nanotubes derived from g-C3N4. Materials (Basel). 13:1349. doi:10.3390/ma13061349.

Meijer BJ, Smit WL, Koelink PJ, Westendorp BF, de Boer RJ, van der Meer JH, Vermeulen JL, Paton JC, Paton AW, Qin J, et al. 2021. Endoplasmic reticulum stress regulates the intestinal stem cell state through CtBP2. Sci Rep. 11:9892. doi:10.1038/s41598-021-89326-w.

Potapov V, Kaplan JB, Keating AE. 2015. Data-driven prediction and design of bZIP coiled-coil interactions. PLoS Comput Biol. 11:e1004046. doi:10.1371/journal.pcbi.1004046.

Qin Y, Zhou Z-W, Pan S-T, He Z-X, Zhang X, Qiu J-X, Duan W, Yang T, Zhou S-F. 2015. Graphene quantum dots induce apoptosis, autophagy, and inflammatory response via p38 mitogen-activated protein kinase and nuclear factor-κB mediated signaling pathways in activated THP-1 macrophages. Toxicology. 327:62–76. doi:10.1016/j.tox.2014.10.011.

Rozpedek W, Pytel D, Mucha B, Leszczynska H, Diehl JA, Majsterek I. 2016. The role of the PERK/eIF2α/ATF4/CHOP signaling pathway in tumor progression during endoplasmic reticulum stress. Curr Mol Med. 16:533–544. doi:10.2174/1566524016666160523143937.

Schröder M, Kaufman RJ. 2005a. ER stress and the unfolded protein response. Mutat Res Fundam Mol Mech Mutagen. 569:29–63. doi:10.1016/j.mrfmmm.2004.06.056.

Schröder M, Kaufman RJ. 2005b. The mammalian unfolded protein response. Annu Rev Biochem. 74:739–789. doi:10.1146/annurev.biochem.73.011303.074134.

Shen H, Gao Q, Zhang Y, Lin Y, Lin Q, Li Z, Chen L, Zeng Z, Li X, Jia Y, et al. 2019. Visible quantum dot light-emitting diodes with simultaneous high brightness and efficiency. Nat Photonics. 13:192–197. doi:10.1038/s41566-019-0364-z.

Song S-Y, Liu K-K, Wei J-Y, Lou Q, Shang Y, Shan C-X. 2019. Deep-ultraviolet emissive carbon nanodots. Nano Lett. 19:5553–5561. doi:10.1021/acs.nanolett.9b02093.

Tsoi KM, Dai Q, Alman BA, Chan WC. 2013. Are quantum dots toxic? Exploring the discrepancy between cell culture and animal studies. Acc Chem Res. 46:662–671. doi:10.1021/ar300040z.

Vimalraj S. 2020. Alkaline phosphatase: Structure, expression and its function in bone mineralization. Gene. 754:144855. doi:10.1016/j.gene.2020.144855.

Wang H, Liu Z, Gou Y, Qin Y, Xu Y, Liu J, Wu J-Z. 2015. Apoptosis and necrosis induced by novel realgar quantum dots in human endometrial cancer cells via endoplasmic reticulum stress signaling pathway. Int J Nanomed. 5505–5512. doi:10.2147/IJN.S83838.

Wang L, Li W, Yin L, Liu Y, Guo H, Lai J, Han Y, Li G, Li M, Zhang J, et al. 2020. Full-color fluorescent carbon quantum dots. Sci Adv. 6:eabb6772. doi:10.1126/sciadv.abb6772.

Wang M, Ren J, Liu Z, Li S, Su L, Wang B, Han D, Liu G. 2022. Beneficial Effect of selenium doped carbon quantum dots supplementation on the in vitro development competence of ovine oocytes. Int J Nanomed. 2907–2924. doi:10.2147/IJN.S360000.

Xiao A, Wang C, Chen J, Guo R, Yan Z, Chen J. 2016. Carbon and metal quantum dots toxicity on the microalgae Chlorella pyrenoidosa. Ecotoxicol Environ Saf. 133:211–217. doi:10.1016/j.ecoenv.2016.07.026.

Yan M, Zhang Y, Qin H, Liu K, Guo M, Ge Y, Xu M, Sun Y, Zheng X. 2016. Cytotoxicity of CdTe quantum dots in human umbilical vein endothelial cells: the involvement of cellular uptake and induction of pro-apoptotic endoplasmic reticulum stress. Int J Nanomed. 529–542. doi:10.2147/IJN.S93591.

Yu L, Tian X, Gao D, Lang Y, Zhang X-X, Yang C, Gu M-M, Shi J, Zhou P-K, Shang Z-F. 2019. Oral administration of hydroxylated-graphene quantum dots induces intestinal injury accompanying the loss of intestinal stem cells and proliferative progenitor cells. Nanotoxicology. 13:1409–1421. doi:10.1080/17435390.2019.1668068.

Zhang D, Zhang Z, Wu Y, Fu K, Chen Y, Li W, Chu M. 2019. Systematic evaluation of graphene quantum dot toxicity to male mouse sexual behaviors, reproductive and offspring health. Biomaterials. 194:215–232. doi:10.1016/j.biomaterials.2018.12.001.

Zhang R, Rapin N, Ying Z, Shklanka E, Bodnarchuk TW, Verge VM, Misra V. 2013. Zhangfei/CREB-ZF–a potential regulator of the unfolded protein response. PLoS One. 8:e77256. doi:10.1371/journal.pone.0077256.

Zhang S, Pei X, Xue Y, Xiong J, Wang J. 2020. Bio-safety assessment of carbon quantum dots, N-doped and folic acid modified carbon quantum dots: a systemic comparison. Chin Chem Lett. 31:1654–1659. doi:10.1016/j.cclet.2019.09.018.

Zhang T, Lu J, Yao Y, Pang YT, Ding XM, Tang M. 2023. MPA-capped CdTequantum dots induces endoplasmic reticulum stress-mediated autophagy and apoptosis through generation of reactive oxygen species in human liver normal cell and liver tumor cell. Environ Pollut. Jun 1;326:121397. doi:10.1016/j.envpol.2023.121397.

Zhou Z, Wang Q, Michalak M. 2021. Inositol Requiring Enzyme (IRE), a multiplayer in sensing endoplasmic reticulum stress. Animal Cells Syst (Seoul). 25:347–357. doi:10.1080/19768354.2021.2020901.

Zielke N, Edgar B. 2015. FUCCI sensors: powerful new tools for analysis of cell proliferation. Wiley Interdiscip Rev Dev Biol. 4:469–487. doi:10.1002/wdev.189.